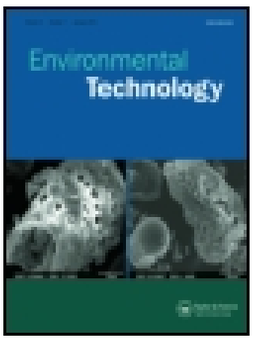

Environmental Technology

ISSN: (Print) (Online) Journal homepage: https://www.tandfonline.com/loi/tent20

Can CO_2 sequestration in basalt efficiently reduce greenhouse gas emission?

Michael O. Schwartz

To cite this article: Michael O. Schwartz (2020): Can CO_2 sequestration in basalt efficiently reduce greenhouse gas emission?, Environmental Technology, DOI: 10.1080/09593330.2020.1815859

To link to this article: https://doi.org/10.1080/09593330.2020.1815859

Published online: 09 Sep 2020.

ENVIRONMENTAL TECHNOLOGY
https://doi.org/10.1080/09593330.2020.1815859

Taylor & Francis
Taylor & Francis Group

Can CO_2 sequestration in basalt efficiently reduce greenhouse gas emission?

Michael O. Schwartz

MathGeol, Langenhagen, Germany

ABSTRACT

The research on the Columbia River Basalt is a unique combination of projects that minimise CO_2 emissions to the atmosphere. Both are underground waste disposal projects: CO_2 waste versus nuclear waste. The recent Wallula CO_2 project and the previous nuclear-waste project in the Columbia River Basalt (CRB), USA, provide the database for a high-capacity CO_2 sequestration model. Due to geomechanical constraints, the injection rate of CO_2 sequestration must be limited in order not to jeopardise the integrity of the reservoir and cap rock. The interbed in the continental flood basalt tested in the Wallula project only allows injection at a rate in the range of 9–19 kg CO_2/s, depending on permeability (4×10^{-14}–10^{-13} m^2) and porosity (0.1–0.15). At the end of a 50-year injection period, the fraction of CO_2 converted to carbonate minerals is 37.1–67.1%. Underground space for waste disposal is a rare asset. The Columbia River Basalt occupies an area of 200,000 km^2. Fifty years of CO_2 sequestration from a single well would require about the same fraction of the area as that of a nuclear waste repository (0.025%). The repository design is for a capacity of 70,000 MTHM (metric tons heavy metal). If all the waste is spent nuclear fuel, it originates from 1.2×10^4–8.4×10^4 TWh electric power production, depending on reactor type. The CO_2 injection well operating at maximum capacity (19 kg CO_2/s) represents 50 TWh generated in a gas power station minus the energy consumed for CO_2 separation, i.e. less than 0.4% of the nuclear option.

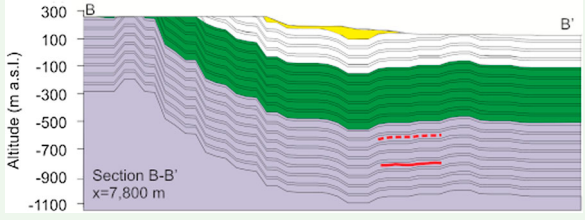

ARTICLE HISTORY
Received 20 April 2020
Accepted 20 August 2020

KEYWORDS
Carbon dioxide; sequestration; basalt; nuclear waste disposal; greenhouse gas

1. Introduction

The separation of carbon dioxide (CO_2) from gas produced in a power station or other industrial source and its subsequent underground storage is a candidate method for the reduction of the emissions of greenhouse gases into the atmosphere. The most frequently proposed procedure is the injection of supercritical CO_2 into a sandstone aquifer. However, this poses a considerable risk that the CO_2 may leak to a near-surface aquifer and pollute the groundwater ([1], and references therein). In a sandstone aquifer, there are hardly any mineral components that react with CO_2 to produce stable carbonate mineral phases within a reasonably short time (<1000 years; [2]). The situation is completely different in basalt aquifers which have become an important research topic in recent years. The overall chemical composition of basalt and its partly non-crystalline (glassy) structure make it an ideal CO_2 trap. This is particularly true for the chemical composition of mid-ocean-ridge basalt (MORB) and, to a lesser degree, for the chemical composition of continental flood basalt (CFB). Much of the injected CO_2 can be fixed in a basalt aquifer within a few years if the CO_2 injection rate is low and the injection time is short. This has been shown in the Hellisheidi pilot project (Iceland) that targeted a MORB aquifer. The CO_2 injection rate in this pilot project is particularly low because CO_2-enriched water was injected instead of the usual supercritical CO_2 [3–5].

The objective of the present work is (1) to investigate the efficiency of industrial-scale supercritical CO_2 injection into an unconventional reservoir and (2) to make CO_2 injection comparable to the competing nuclear energy strategy. Both strategies suffer from the scarcity of suitable

CONTACT Michael O. Schwartz mathgeol@yahoo.de MathGeol, Postfach 101204, Langenhagen 30833, Germany

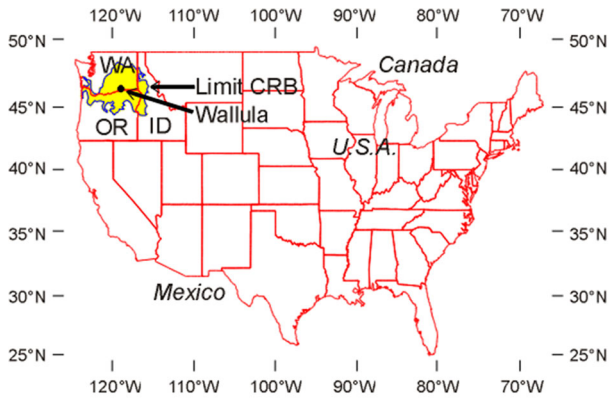

Figure 1. Extent of the Columbia River Basalt (CRB) and location of the Wallula pilot project.

target rock and low public acceptance. This paper presents a completely novel approach to the climate change problem. The test situation in the CFB-type Columbia River Basalt (CRB), USA., (Figure 1) is almost ideal. In the period from 1968 to 1987, the CRB hosted a high-level nuclear waste project [6–9]. From 2011 to 2015, the CRB hosted the Wallula pilot project during which supercritical CO_2 was injected at a rate of 0.46 kg CO_2/s for a period of 25 days [10]. The Wallula project was technically successful but lagged behind the Hellisheidi project in terms of the all-important monitoring of fluid evolution. The Hellisheidi project had a monitoring well down-gradient from the injection well while no monitoring well was included in the Wallula project. To fill this information gap, it was necessary to set up a novel geochemical modelling procedure and calibrate it using the monitoring results of the Hellisheidi project (Figure 2).

2. Materials

2.1. Data base

The base-case model is designed to be a real-world example with industrial dimensions of a so-called unconventional reservoir [11]. The injection rates are in the range of 9–19 kg CO_2/s. The injection time of fifty years corresponds to the maximum lifetime that can be expected from a metallic installation used for injecting corrosive CO_2. The 50-year period approximately coincides with the production of 70,000 MTHM (metric tons of heavy metal, including uranium and other heavy metal) in the USA. This statuary limit is specified by the Nuclear Waste Policy Act of 1982 for the first high-level repository in the USA.

The injection depth is set at 850 m and the in situ temperature is 40°C (Table 1). The target horizon is a 20 m thick interbed in the Grande Ronde Basalt (GRB) that has an age of 15.6–16.5 Ma and forms a part of the Columbia River Basalt Group (6–17.5 Ma; [12]). The target horizon has an effective porosity in the range of 0.1–0.15 [12, 13]. The minimum porosity value is taken as the base-case value. The permeability is in a relatively narrow range (from 4×10^{-14} to 1×10^{-13} m^2) according to the data from the Wallula borehole [13], and an intermediate value (7×10^{-14} m^2) is taken as the base-case value. It is noted that the permeability of the CRB interbeds varies in a much wider range than the values from the Wallula borehole [12, 14, 15] and there is a considerable uncertainty with respect to the rock properties beyond the Wallula borehole. The target horizon is overlayed and underlayed by basalt. The permeability of basalt is low (10^{-21}–10^{-17} m^2; [12, 16]). The maximum value is taken as the base-case value, and the effective porosity is set to 0.005 in agreement with a previous model [9].

The major element concentrations, pH and the Eh value of the GRB groundwater are the average values of Reidel et al. [12], excluding Si and Al (averages for the CRB Group in Washington; [20]) (Table 2). The major element concentrations of GRB pillow lava glass (Table 3) are the averages of Mangan et al. [21].

The stress regime and rock properties of the GRB are identical to those determined in the nuclear waste

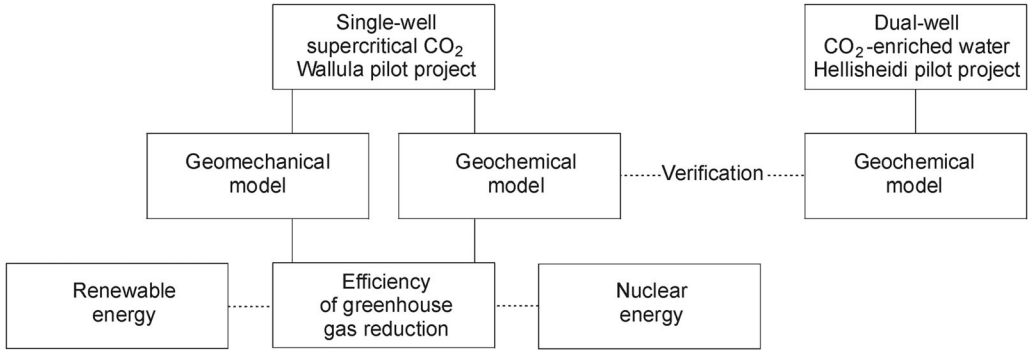

Figure 2. Model flowchart.

repository project. Rock density is 2800 kg/m^3, Young's modulus is 67.8 GPa, Poisson's ratio is 0.26, thermal expansion is 7.45×10^{-6} K^{-1}, specific heat capacity is 950 J m^{-3} K^{-1}, and thermal conductivity is 2.3 W m^{-1} K^{-1} [6]. The ratio between vertical stress, minimum horizontal stress and maximum horizontal stress is 1:1.32:2.34 [18].

The Wallula pilot project that targeted CFB contains only one injection well but no monitoring wells. Therefore, it is not possible to directly compare the model results with empirical results. However, the other basalt project located in MORB at Hellisheidi, Iceland, contained a monitoring well in addition to the injection well. Although there are differences in the reservoir rock composition and injection method, the data from Hellisheidi are suitable for adaption to enable indirect comparison with the Wallula project.

Table 1. Flow and geomechanical model setup.

General properties	
Model length/width/height (km)	10/10/1
Top elevation (km)	0.35
Bottom elevation (km)	1.35
Injection depth (km)	0.85
Top pressure (MPa)	3.5
Injection rate (kg/s)	9–19
Injection period (a)	50
Reservoir temperature (°C)	40
Injection temperature (°C)	40
Initial saturation (-)	1
Unsaturated hydraulic properties	
Residual liquid saturation (-)	0
Residual gas saturation (-)	0
van Genuchten parameter α (MPa)[a]	0.01961
van Genuchten parameter m (-)[a]	0.457
Rock properties	
Initial porosity (-)[b]	0.005–0.15
Initial permeability (m^2)[c]	10^{-17}–10^{-13}
Thermal conductivity (W m^{-1} K^{-1})[d]	2.3
Rock grain density (kg/m^3)[d]	2800
Specific heat capacity (J m^{-3} K^{-1})[d]	950
Coefficient of thermal expansion (K^{-1})[d]	7.45×10^{-6}
Young's modulus (GPa)[d]	67.8
Poisson's ratio (-)[d]	0.26
Biot's coefficient (-)	0.5
Fracture properties	
Maximum horizontal/vertical stress ratio[e]	2.34
Minimum horizontal/vertical stress ratio[e]	1.32
Fractures per control volume[f]	100
d_5 (mm)[g]	1
d_{95} (mm)[g]	3.5
Maximum increase in permeability[f]	50
Cohesion (MPa)[f]	2.7
Static friction coefficient (-)[f]	0.65
Dynamic friction coefficient (-)[f]	0.55
Shear fracture stiffness (MPa/m)[f]	500

[a][17].
[b][9,12,13].
[c][12,13].
[d][6].
[e][18].
[f][19].
[g]d_5 and d_{95} are shear displacements at which 5 and 95 %, respectively, of total permeability enhancement occurs [19].

2.2. Computer codes

The flow and transport simulations are performed using the TOUGHREACT code (version 3) while the uncoupled hydraulic-fracturing simulations are carried out with the FEHM code (https://github.com/lanl/FEHM). The FEHM and TOUGHREACT codes are an appropriate match for structured orthogonal grids such as those used in this work.

2.2.1. FEHM

The FEHM code (https://github.com/lanl/FEHM; [22]) is designed for geomechanical CO_2 sequestration problems [23, 24] and geothermal problems [19]. The code calculates the stress-related permeability changes according to the permeability model 25 [19]. Mohr-Coulomb failure criteria are applied to an ensemble of fractures with orientations distributed according to fracture orientation data. The pre-failure increase in permeability occurs according to the model of Bai et al. [25]. The post-failure increase in permeability occurs according to an empirical model based on the work of Lee and Cho [26].

Shear failure occurs due to pressure increases during well-bore injection when shear stress exceeds a frictional threshold. Permeability is allowed to increase wherever the threshold is exceeded. The resulting permeability distribution is more complex than those obtained by the industry-standard design models based on a planar geometry [27–29]. The ovoid distribution patterns are comparable to those obtained by the wire-mesh method [30–33] but are only an approximate equivalent to those obtained using a discrete fracture network (DFN) model [34,35]. The FEHM code uses an approximation procedure by considering an ensemble of fracture systems and allows computation of an upscaled continuum permeability of the fracture population without resorting to an explicit DFN approach [19].

The FEHM program is a control volume finite element (CVFE) code [36]. The structured orthogonal grid used in

Table 2. Chemical composition of continental flood basalt (CFB) groundwater.

pH[a]	9.4
Eh (mV)[a]	−300
Al (mg/L)[b]	0.031
C (mg/L)[a]	17.4
Ca (mg/L)[a]	2.0
Cl (mg/L)[a]	228.4
Fe (mg/L)[a]	0.2
K (mg/L)[a]	10.3
Mg (mg/L)[a]	0.1
Na (mg/L)[a]	246.2
Si (mg/L)[b]	23.9

[a][12].
[b][20].

Table 3. Chemical composition of basalt glass (weight %)

	CFB[a]	MORB[b]
SiO_2	55.00	48.12
Al_2O_3	13.36	14.62
FeO (total Fe)	10.81	10.82
MgO	3.64	9.08
CaO	7.64	11.84
Na_2O	2.83	1.97
K_2O	1.46	0.29

aContinental flood basalt (CFB) pillow lava glass, Grande Ronde Basalt, USA [21].
[b]Mid-ocean ridge basalt (MORB) glass, Stapafell, Iceland [52].

the applications of this paper makes the CVFE method equivalent to the integral finite difference (IFD) method of TOUGHREACT (see the following subsection).

2.2.2. TOUGHREACT

TOUGHREACT version 3 is a numerical simulation programme for the study of chemically reactive non-isothermal flows of multi-phase fluids in porous and fractured media [37]. The programme was developed by introducing reactive chemistry into the multi-phase flow code TOUGH2 [38]. TOUGHREACT handles unsaturated conditions and phase partitioning within the fluids in the same manner as the TOUGH2 code. Interactions between mineral assemblages and fluids can occur under local equilibrium or kinetic rates. The chemically active phases are aqueous liquid, aqueous vapour, CO_2 vapour, CO_2 liquid and supercritical CO_2. Precipitation and dissolution reactions can change the formation porosity and permeability. The governing equations are discretised using integral finite difference for space and fully implicit first-order finite difference for time. All of the simulations carried out in this study were performed with the ECO2N module [39], which is a modified version of the ECO2 module [40]. The reaction rate is a function of the mineral saturation ratio and is calculated using the rate expression of Lasaga et al. [41].

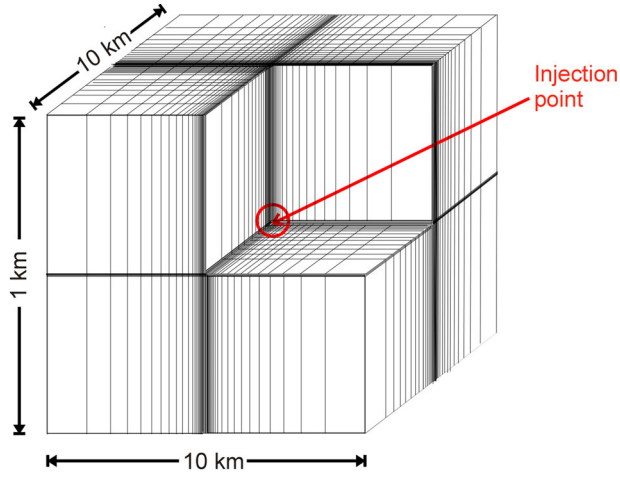

Figure 3. Model mesh.

3. Method

3.1. Geomechanical model set-up

The structured orthogonal model mesh contains 69,192 nodes and has the dimensions of $10 \times 10 \times 1$ km (Figure 3). The top of the mesh is located at a depth of 0.35 km and the injection point is at the centre of the mesh. The horizontal nodal distances at the centre of the mesh are 5 m, and increase logarithmically in the x and y directions with increasing distance from the centre. Up to 10 m above the injections point, the nodal distances in the z direction are 1.43 m, followed by the distances of 20 and 470 m. Below the injection point, the nodal distances are 1.43 m down to 10 m below the injection point, followed by a distance of 490 m.

The hydrological boundaries are defined by a constant pressure corresponding to the hydrostatic fluid pressure (3.5 MPa) at the top of the model and no-flow conditions at the remaining boundaries. The stress boundaries allow displacement at the top as well as on the x and y sides of the model.

The unsaturated flow conditions are calculated using a linear relative-permeability relationship:

- The relative liquid permeability increases from zero to unity in the liquid saturation range of 0–1
- The relative gas permeability increases from zero to unity in the gas saturation range of 0–1.

The non-linear relative permeability relationship of Corey [42] that satisfactorily reproduces the experiments with basalt of Bertels et al. [43] was also tested. These scoping calculations show that the Corey [42] function produces slightly different results. The differences are negligible considering that the convergence behaviour of the code is far inferior compared to the simulations with a linear relationship.

The capillary pressure is calculated with the function of van Genuchten [44] using parameters from a CO_2 sequestration test case reported by Xu et al. [17]. It is theoretically possible to calculate the parameters using the experimental data for basalt [43] but the scatter of such data is so wide that they are hardly suitable for a regression analysis.

The fracture properties are taken from Dempsey et al. [19] except for Young's modulus, Poisson's ratio and horizontal stress that are taken from the nuclear waste project (Table 1). The vertical stress is the lithostatic

stress, and the minimum and maximum horizontal stresses are located parallel to the x and y-axes, respectively. The model is initialised with a high-permeability (10^{-12} m^2) pre-run, during which the pressure is allowed to adjust to the hydrostatic pressure under stress-free conditions. The model is isothermal (40°C).

3.2. Reactive transport model set-up

The uncoupled reactive transport model has the same injection point and the same limits as those of the geomechanical model, and the initialisation pre-run is conducted in the same manner. However, the mesh with 160,000 elements lacks the spatial discretisation near the centre of the mesh. The horizontal nodal distances are 50 m. The central layer has a thickness of 20 m, and is sandwiched by a 480 m-thick and a 10 m-thick layer above and a 490 m-thick layer below. The top layer serves to maintain constant pressure and consists exclusively of infinite-volume boundary elements (10^{52} m^3). These elements impose the Dirichlet conditions, i.e. the thermodynamic properties do not change. After the initialisation pre-run, the volume of the lateral boundaries is increased to 10^{52} m^3, i.e. Dirichlet conditions are imposed. This is equivalent to modelling a laterally infinite reservoir. The model is isothermal (40°C) and the parameters for relative permeability and capillary pressure are the same as those used for the geomechanical model (Table 1).

A mesh with the nodal position of the geomechanical model (5 m horizontal spacing increasing logarithmically) has also been tested. These scoping calculations produce nearly identical results but the convergence behaviour of the TOUGHREACT code is far inferior.

It is noted that a fractured porous media system would be a better alternative than the single porosity system used in this study. However, there is a complete lack of data on fracture spacing in the interbeds of the Columbia River Basalt. Even if such data would be available, the calibration of a suitable multi-continuum model would be a highly complex task requiring several submodels [45,46] and is beyond the scope of this paper.

3.2.1. CFB base case

CFB magma has a mantle source contaminated with continental lithosphere and shows features of magmatic differentiation. Compared to MORB, CFB has relatively high Na and K concentrations as well as low Ca and Mg concentrations. The base case uses CFB.

The transport conditions are simulated in a batch reactor with the Grande Ronde Basalt (GRB) pillow lava glass similar to the one described by Pollyea and Rimstidt [47]. The simulation predicts the behaviour of basalt glass and solution in a 1 m × 1 m × 1 m grid cell packed with grains of 0.3 mm radius; this configuration results in an initial reactive surface area of 10^4 m^2/m^3. The initial water composition is that of the average values of the GRB water, supplemented by the Si and Al values for the CRB Group (Table 2). The concentration of aqueous O_2 is calculated using the actual pH and Eh values. However, the initial H^+ concentration is higher (neutral pH). This is a common approach for initialising a TOUGHREACT model because the calculations are more likely to converge if the pH is set below the expected final value.

Basalt glass is allowed to react with this initial water for a period of 1000 years at 40°C and 8.5 MPa. The basalt glass has the composition of GRB glass normalised to one Si atom (Table 3). A simplified set of reaction products [47], namely calcite, siderite and magnesite, (i.e. carbonates representative of ankerite-dolomite solid solution; [48], amorphous SiO_2, Ca-montmorillonite, Na-montmorillonite and illite, (i.e. Al-silicates representative of mixed-layer minerals solid solution; [49] is used. Kinetic data are not available for solid solutions; therefore, the available data for minerals with a fixed composition must be used. Calcite is set at equilibrium with the fluid phase as a proxy for the extremely high reaction rate. Basalt glass [47], siderite [50] and the remaining components [51] react under kinetic constraints. Illite is assumed to have the same rate constants as montmorillonite. Basalt glass can only dissolve whereas the remaining solid phases can both dissolve and precipitate. The initial volume fraction of basalt glass is 0.1. The initial volume fraction of the remaining crystalline components (composite basalt) is set to zero. This is justified because the dissolution fluxes of composite basalt are several orders of magnitude lower than those of basalt glass (Figure 2 in[47]). The reactive surface area is 10^4 m^2/m^3, identical to that used in the batch reactor for all components reacting under kinetic constraints (Table 4). Both the volume fraction and reactive surface area in this model setup is not critical because differences cancel out in the calibration step described below.

The initial porosity is set at 0.1 for the base case (GRB interbed in the Wallula borehole; [13]) and 0.15 for sensitivity cases, in agreement with the modelling of the gas storage capacity of the total CRB Group, comprising the GRB and overlying formations [12].

The calculations are performed with the THERMODDEM thermodynamic database [53] that is commonly used for TOUGHREACT simulations supplemented by the data for basalt glass, and using all aqueous species of the elements shown in Table 2. The equilibrium constant for basalt glass dissolution at 40°C ('*K*'), which is not known a priori, is a convenient fitting parameter.

Table 4. TOUGHREACT flow-transport model setup: Initial volume fractions, reactive surface areas and kinetic properties.

Mineral/rock	Chemical composition	Initial	Reactive volume surface fraction area (m^2/m^3)					
Calcite (equilibrium)	$CaCO_3$	0.0	-					
Amorphous SiO_2	SiO_2	0.0	10,000					
Illite	$K_{0.85}Si_{3.15}Al_{2.85}O_{10}(OH)_2$	0.0	10,000					
Siderite	FeCO3	0.0	10,000					
Magnesite	$MgCO_3$	0.0	10,000					
Ca-montmorillonite	$Ca_{0.17}Al_{1.68}Mg_{0.33}Si_{3.99}O_{10}(OH)_2$	0.0	10,000					
Na-montmorillonite	$Na_{0.33}Al_{1.67}Mg_{0.33}Si_4O_{10}(OH)_2$	0.0	10,000					
CFB glass	$SiAl_{0.286}Fe(II)_{0.164}Mg_{0.094}Ca_{0.149}Na_{0.100}K_{0.034}O_{2.903}$	0.05–0.1	10,000					
MORB glass	$SiAl_{0.358}Fe(II)_{0.189}Mg_{0.281}Ca_{0.264}Na_{0.079}K_{0.008}O_{3.315}$	0.05–0.1	10,000					
	Rate parameters[a]							
	Acid mechanism	Neutral mechanism	Base mechanism					
Mineral/rock	k_{25} (mol/m^2/s)[b]	E_a (KJ /mol)[b]	n(H^+)[b]	k_{25} (mol/m^2/s)	E_a (KJ/mol)[b]	k_{25} (mol /m^2/s)	E_a (KJ/mol)	n(H^+)
Amorphous SiO_2	-	-	-	5.89×10^{-13}	74.5	-	-	
Illite	1.95×10^{-13}	48.0	0.22	3.89×10^{-15}	48.0	3.89×10^{-15}	48.0	−0.13
Siderite	9.77×10^{-4}	20.9	0.90	1.26×10^{-9}	62.8	-	-	-
Magnesite	4.17×10^{-7}	14.4	1.00	4.57×10^{-10}	23.5	6.02×10^{-6}	62.8	1.00
Montmorillonite	1.95×10^{-13}	48.0	0.22	3.89×10^{-15}	48.0	3.89×10^{-15}	48.0	−0.13
Glass	5.37×10^{-5}	39.7	1.01	-	-	1.00×10^{-11}	38.4	−0.26

[a] Parameters for mineral dissolution and precipitation.
b k25 is the kinetic rate constant at 25°C; E_a is the Arrhenius activation energy; n(H^+) is the reaction order with respect to H+.

The difference between the actual and predicted concentration is minimised by varying '*K*' with small steps ($\log\Delta_K = 0.05$). The fitting is performed by minimising the difference $|d_{min}|$:

$$\log(d_{min}) = \sum \log(c_{p,i}) - \sum \log(c_{a,i}), \quad (1)$$

where '$c_{p,i}$' is the predicted concentration of component '*i*' and '$c_{a,i}$' is the actual concentration of component '*i*' that refers to the composition of GRB groundwater, excluding pH and Eh. The fitting procedure yielded log (*K*) = 3.85 (Figure 4). The predicted pH of 9.519 is only slightly different from the actual pH (9.4). Thus, log(*K*) = 3.85 is used for all simulations with CFB.

The simulation period is 50 years. The injections rates are 280,000 and 600,000 t CO_2/a, representing the lower threshold (9 kg CO_2/s) and upper threshold (19 kg CO_2/s), respectively, in the geomechanical model (Table 5). The porosity-permeability relationship is defined by the cubic law. Diffusivity is zero for all aqueous species.

3.2.2. MORB sensitivity case

Instead of using CFB glass normalised to one Si atom, normalised MORB glass [52] is used in the batch reactor. The initial fluid composition and the fitting procedure are identical to those used for the CFB base case (Table 2). The best-fit log(K) value of 8.95 produces a pH of 9.765, which is significantly above the average pH (9.4) of GRB groundwater. Note that for a theoretical reference fluid with the composition of MORB groundwater (e.g.

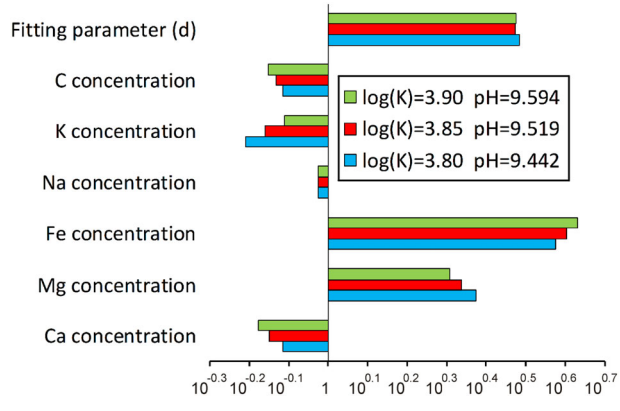

Figure 4. Continental flood basalt (CFB) model**.** Ratios between predicted and actual concentration of major elements in groundwater of the Grande Ronde Basalt (GRB) for various equilibrium constants for GRB glass dissolution. The fitting parameter '*d*' is also shown. See text for explanation.

Table 5. FEHM geomechanical model.

Permeability (m^2)	Porosity (-)	Threshold CO_2 injection rate (kg/s)[a]
10^{-13}	0.15	19.0
10^{-13}	0.1	17.5
7×10^{-14}	0.15	14.5
7×10^{-14}	0.1	13.0
4×10^{-14}	0.15	10.0
4×10^{-14}	0.1	9.0

[a]Threshold at which shear stress-related permeability enhancement occurs.

Table 3 in [54]), the agreement between actual pH (9.26) and predicted pH (9.613) will not be better and the comparability between MORB glass and CFB glass will be lost in this case.

4. Results

4.1. Base case

4.1.1. Geomechanical model

The base-case permeability (7×10^{-4}) and base-case porosity (0.1) allow an injection rate of up to 13 kg CO_2/s before the reservoir rock starts to lose its mechanical integrity. This is monitored by the onset of permeability increase when the shear stress exceeds the frictional threshold ('Geomechanical model set-up'; Table 5). Above the threshold, the permeability increases at the injection point and the surrounding nodes occur in a relatively short time (less than 10 days).

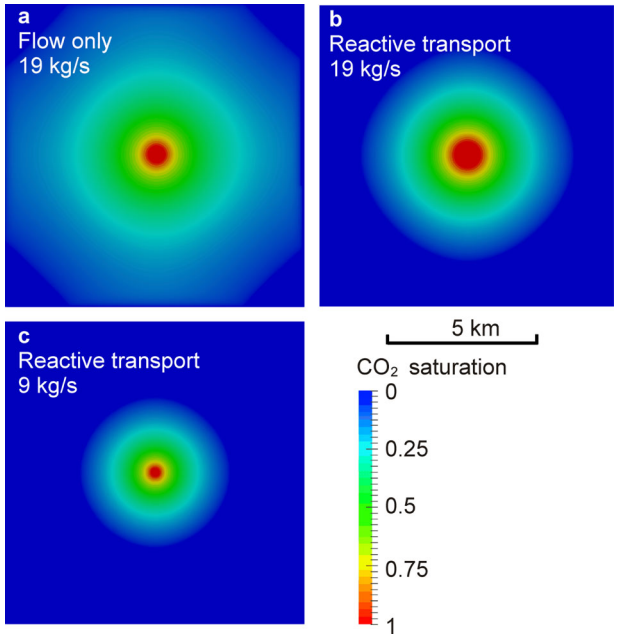

Figure 5. Continental flood basalt (CFB) model**.** CO_2 gas saturation after 50 years of CO_2 injection into a 20-m thick interbed in the Grande Ronde Basalt (GRB). **A** Map showing non-reactive flow for an injection rate of 19 kg CO_2/s. **B** Map showing reactive-transport for an injection rate of 19 kg CO_2/s. **C** Map showing reactive-transport for an injection rate of 9 kg CO_2/s.

4.1.2. Reactive-transport model

At the end of the 50-year injection period, the diameter of the CO_2 plume (one-phase supercritical CO_2 and two-phase CO_2/H_2O) is 4.8 and 6.9 km for the reactive transport model with the injection rates of 9 and 19 kg CO_2/s, respectively (Figure 5). The reaction products within 10 days of arrival of the CO_2 plume are calcite followed by siderite and magnesite (i.e. carbonates representative of ankerite-dolomite solid solution), amorphous silica, montmorillonite and illite (i.e. Al-silicates representative of mixed-layer minerals solid solution).

The pH of the fluid is in the range of 5–5.6 within the CO_2 plume prior to the onset of large-scale secondary mineral precipitation. The pH stabilises in a narrow range (9.0– 9.8) after the onset of large-scale secondary mineral precipitation (Figure 6); i.e. the pH is close to the pre-injection pH (9.4). The pH rises to above 10

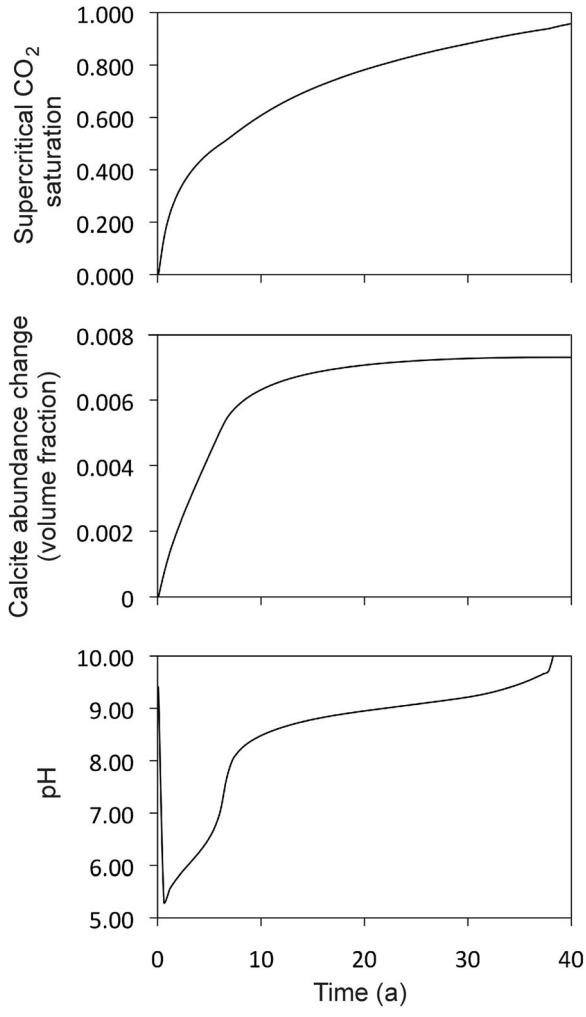

Figure 6. Continental flood basalt (CFB) model. Liquid saturation, calcite volume change and pH versus time at 400 m distance from the CO_2 injection point. The injection rate is 19 kg CO_2/s, the permeability is 7×10^{-14}, the porosity is 0.1 and the volume fractions of basalt glass is 0.1.

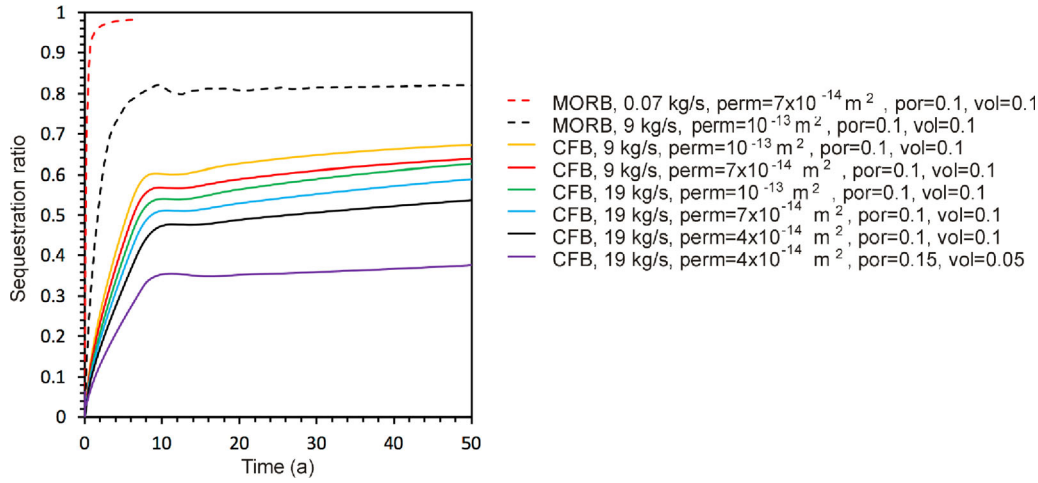

Figure 7. Mid-ocean-ridge basalt (MORB) and continental flood basalt (CFB) model. CO_2 sequestration ratios versus time for various CO_2 injection rates (0.07, 9 and 19 kg CO_2/s). The permeabilities (perm) are 4×10^{-14}, 7×10^{-14} and 10^{-13} m^2. The porosities (por) are 0.1 and 0.15. The volume fractions of basalt glass (vol) are 0.05 and 0.1.

only close to the outer limit of the CO_2 plume. When all basalt glass has dissolved in the late injection stages, the pH tends to approach a value of 5 within the CO_2 plume.

The fraction of CO_2 fixed in precipitated carbonated phases decreases with increasing injection rate. The fraction of sequestered CO_2 at the end of the injection period is 62.0% and 58.6% for the injection rates of 9 and 19 kg CO_2/s, respectively (Figure 7).

The maximum injection rate of 19 kg/s is a theoretical value that is difficult to achieve in practice (Table 5). Reducing the injection rate to 9 kg CO_2/s has the additional advantage that the fraction of sequestered CO_2 is increased.

In a flow-only model, i.e. in a model that does not include chemical reactions, the diameter of the CO_2 plume is much larger than that in a model that includes chemical reactions. For example, the plume is simulated to extend by approximately 60% with respect to the corresponding reactive-transport model, i.e. beyond the boundaries of the 10 km-diameter model, at an injection rate of 19 kg CO_2/s (Table 6).

4.2. Sensitivity cases

4.2.1. Geomechanical model

The geomechanical risk increases with the decreasing permeability and porosity of the reservoir rock, in addition to the risks related to an injection rate increase (Table 5). The pessimistic case with a permeability of 4×10^{-14} m^2 and porosity of 0.1 only allows an injection rate of 9 kg CO_2/s without producing permeability changes or damaging the reservoir rock and jeopardising the integrity of the cap rock. The optimistic case with a permeability of 10^{-13} m^2 and porosity of 0.15 allows an injection rate of up to 19 kg CO_2/s without producing permeability changes.

4.2.2. Reactive-transport model

The sensitivity tests address some important uncertainties in the simulations results:

- agreement with experimental data
- influence of the composition of the aquifer
- influence of the permeability of the aquifer
- influence of the porosity of the aquifer
- influence of the volume fraction of basalt glass in the aquifer.

The first sensitivity test evaluates the accuracy of the base case simulations by comparison to the experimental data. The CFB project is not suitable for such a comparison because it contained only an injection well and no monitoring wells. By contrast, the MORB project at Hellisheidi, Iceland, monitored the fluid evolution in an additional monitoring well (see 'Introduction'). CO_2-enriched water was injected at Hellisheidi at a rate

Table 6. TOUGHREACT geochemical model. CO_2 sequestration ratios (%) after 4 and 50 years (in parentheses) injection into basalt with a porosity of 0.1 and a glass volume fraction of 0.1.

	Permeability (m^2)		
	4×10^{-14}	7×10^{-14}	10^{-13}
CFB injection rate = 9 kg/s		37.1 (62.0)[a]	40.8 (67.1)
CFB injection rate = 19 kg/s	27.4 (53.6)	31.0 (58.6)[b]	33.7 (62.2)
MORB injection rate = 0.07 kg/s		97.6	
MORB injection rate = 9 kg/s			70.4 (81.9)

[a]The diameter of the CO_2 plume (one-phase supercritical CO_2 and two-phase CO_2/H_2O) is 4.8 km after 50 years CO_2 injection.
[b]The diameter of the CO_2 plume is 6.9 km after 50 years CO_2 injection.

corresponding to 0.07 kg CO_2/s, and the chemical evolution of the groundwater was continuously monitored for an additional 15 months until the submersible pump broke down. The injected CO_2-enriched water was originally spiked with carbon isotopes. Based on the final carbon isotope ratios of the groundwater, 95–98% of the injected CO_2 was converted to carbonate minerals.

Modelling the MORB experiment by using supercritical CO_2 instead of CO_2-enriched water results in the sequestration ratios of 95% and 98% after 1.5 and 4 years, respectively. The agreement between the model and experiment results appears to be better than that of an older model with crystalline basalt that calculates that 80% of the injected CO_2 is mineralised in 5 years [55]. Thus, the simulation procedure used in this paper is at least as efficient as that used in the previous modelling study.

The second sensitivity test uses Grande Ronde basalt glass with the composition of MORB glass, instead of the actual CFB glass. This test shows the strong influence of the aquifer composition. The 50-year CFB model with an injection rate of 9 kg CO_2/s and a permeability of 10^{-13} m^2 allows 67.1% of the injected CO_2 to be fixed as solid carbonate phases, whereas the MORB model predicts 81.9%.

The third sensitivity test uses different permeabilities. This test shows that the permeability of the aquifer strongly influences the sequestration ratio. Injecting CO_2 into CFB at a rate of 19 kg/s results in 62.2% sequestration if the permeability is as high as 10^{-13} m^2. The pessimistic case with a permeability of 4×10^{-14} m^2 allows only 53.6% sequestration.

The last sensitivity test shows the combined effect of the variations of the CFB porosity and volume fraction of the CFB glass. This effect is observed in the late sequestration stages when basalt glass completely dissolves locally. The CO_2 sequestering capacity of the reservoir depends on the concentration of the elements in the aquifer that are capable of forming carbonates by fluid-solid reactions (mainly Ca, Mg and Fe), and the kinetic instability of the rock. Crystalline phases are much less reactive than metastable amorphous phases such as basalt glass. There is strong evidence that groundwater chemistry is mainly controlled by the composition of the glass phase whereas the role of crystalline phases is minor or, at the very least is difficult to capture by geochemical modelling [47]. Replacing the base-case porosity of the reservoir rock (0.1) and glass volume fraction (0.1) by the values of 0.15 and 0.05, respectively, strongly reduces carbonate precipitation. The CFB model with an injection rate of 19 kg CO_2/s and permeability of 4×10^{-14} m^2 will have a sequestration ratio of 37.1% instead of 53.6%. For MORB, the corresponding sequestration ratios would be 49.7% and 71.8%.

5. Discussion and conclusion

The research on Columbia River Basalt is a unique combination of projects for the minimisation of CO_2 emissions into the atmosphere. Both are underground waste disposal projects: CO_2 waste versus nuclear waste. Each project targets the high-pH groundwater regime, albeit for different reasons. For CO_2 sequestration, reactivity (between carbon species and calcium, magnesium and iron species) is desirable. For nuclear waste disposal, it is just the opposite, i.e. the non-reactivity between groundwater and the metallic waste container is desirable.

Underground space for waste disposal is a rare resource. The Columbia River Basalt occupies an area of 200,000 km^2. Fifty years of CO_2 sequestration from a single well will require approximately the same fraction of the area as that of a nuclear waste repository (0.025%). The repository design is for a capacity of 70,000 MTHM (metric tons of heavy metal, including uranium and other radioactive metals). If all of the waste is spent nuclear fuel, it originates from 1.2×10^4 to 8.4×10^4 TWh electric power production, depending on the reactor type [56]. The CO_2 injection well operating at maximum capacity (19 kg CO_2/s) represents 50 TWh generated in a gas power station minus the energy consumed for CO_2 separation, i.e. less than 0.4% of the nuclear option.

Both for CO_2 sequestration and nuclear waste disposal, it is problematic to increase the storage volume vertically, albeit for different reasons. Stacking CO_2 sequestration levels increases the geomechanical risk. Stacking nuclear waste repository levels is less efficient than horizontal expansion. The dissipation of radioactive heat is easier to control horizontally than vertically because of the upward movement of heated groundwater. In summary, the Columbia River Basalt projects have the merit of juxtaposing the two most important concepts of greenhouse gas control for non-renewable energy generation. The selected localities are among the best that geology can offer. The CO_2 option has the advantage of minor technical risk but the disadvantage of major space consumption. The nuclear option has the disadvantage of major technical risk but the advantage of minor space consumption.

Can CO_2 sequestration in basalt efficiently reduce greenhouse gas emission? The answer is 'Yes' for supercritical CO_2 with a note of caution. As long as nuclear energy is not replaced by renewable energy, there remains an ethical problem. The only known geological

environment where nuclear waste can be stored under conditions of thermodynamic equilibrium is represented by basaltic rocks [46]. It is unethical to squander valuable underground space as long as we do not know how much will be needed for the disposal of nuclear waste. Another aspect is economics. Coal/hydrocarbon energy linked to CO_2 sequestration must compete with renewable energy. New wind farms in the North Sea already operate without state subsidies [57]. The typical tectonic setting of basalt provinces is quite different from that of coal/hydrocarbon basins. This implies particularly long distances for CO_2 pipeline transport in the case of coal power stations. Hydrocarbon energy offers greater logistical flexibility but competition from renewable energy is a steadily increasing handicap for its use [58].

Disclosure statement

No potential conflict of interest was reported by the author.

References

[1] Schwartz MO. Modelling leakage and groundwater pollution in a hypothetical CO_2 sequestration project. Int J Greenhouse Gas Control. 2014;23:72–85.

[2] Gilfillan SMV, Lollar BS, Holland G, et al. Solubility trapping in formation water as dominant CO_2 sink in natural gas fields. Nature. 2009;458:614–618.

[3] Sigfusson B, Gislason SR, Matter JM, et al. Solving the carbon-dioxide buoyancy challenge: The design and field testing of a dissolved CO2 injection system. Int J Greenhouse Gas Control. 2015;37:213–219.

[4] Matter JM, Stute M, Snaebjornsdottir SO, et al. Rapid carbon mineralization for permanent disposal of anthropogenic carbon dioxide emissions. Science. 2016;352:1312–1314.

[5] Gunnarsson I, Aradóttir ES, Oelkers EH, et al. The rapid and cost-effective capture and subsurface mineral storage of carbon and sulfur at the CarbFix2 site. Int J Greenhouse Gas Control. 2018;79:117–126.

[6] DOE. Site characterization report for the basalt waste isolation project. Washington, D.C., U.S.A.: US Department of Energy (DOE) DOE/RL 82-3, Volume I and Volume II; 1982.

[7] DOE. Site characterization plan. Washington, D.C., U.S.A.: US Department of Energy (DOE) DOE/RW-0164; 1988.

[8] Schwartz MO. The new wallula CO_2 project may revive the old Columbia river basalt (western USA) nuclear-waste repository project. Hydrogeol J. 2018;26:3–6.

[9] Schwartz MO. Modelling groundwater contamination above a potential nuclear waste repository in the Columbia river basalt, USA. Environ Earth Sci. 2018;77:451. doi:10.1007/s12665-018-7615-z.

[10] McGrail BP, Schaef HT, Spane FA, et al. Wallula basalt pilot demonstration project: post-injection results and conclusions. Energy Procedia. 2017;114:5783–5790.

[11] Jones KB, Blondes MS. Carbon dioxide storage in unconventional reservoirs workshop: summary of recommendations. Washington, D.C., U.S.A.: U.S. Geological Survey Open-File Report 2015-1079; 2015.

[12] Reidel SP, Johnson VG, Spane FA. Natural gas storage in basalt aquifers of the Columbia basin, pacific northwest USA: a guide to site characterization. Richland, Washington, USA: PNNL-13962, Pacific Northwest National Laboratory; 2002.

[13] McGrail BP, Spane FA, Sullivan EC, et al. The wallula basalt sequestration pilot project. Energy Procedia. 2011;4:5653–5660.

[14] Jane RS, Pollyea RM. Permeability correlation structure of the Columbia river plateau and implications for fluid system architecture in continental large igneous provinces. Geology. 2018;46:715–718.

[15] Jane RS, Wu H, Pollyea RM. Geologic CO_2 sequestration and permeability uncertainty in a highly heterogeneous reservoir. Int J Greenhouse Gas Control. 2019;83:128–139.

[16] Burns ER, Williams CF, Ingebritsen SE, et al. Understanding heat and groundwater flow through continental flood basalt provinces: insights gained from alternative models of permeability/depth relationships for the Columbia plateau, USA. Geofluids. 2015;15:120–138.

[17] Xu T, Sonnenthal E, Spycher N, et al. TOUGHREACT v3.0-OMP sample problems. Berkeley (USA): Earth Sciences Division, Lawrence Berkeley National Laboratory; 2014.

[18] Haimson BC. Stress measurements at Hanford, Washington, for the design of a nuclear waste repository facility). Proceedings of the Sixth International Congress on rock Mechanics; Montreal, Canada, 30 August– 4 September 1987, p.119–124.

[19] Dempsey D, Kelkar S, Lewis K, et al. Modeling shear stimulation of the desert peak EGS well 27-15 using a coupled thermo-hydrological-mechanical simulator. ARMA. 2013;13-608.

[20] Newcomb RG. Quality of the ground water in basalt of the Columbia river group. Washington, Oregon and Idaho: U.S. Geological Survey Water-Supply Paper 1999-N; 1972.

[21] Mangan MT, Wright TL, Swanson DA, et al. Major oxide, trace element, and glass chemistry pertinent to regional correlation of grande ronde basalt flows, Columbia river basalt group. Washington: U.S. Geological Survey Open-File Report; 1985; p. 85–747.

[22] Zyvoloski GA, Robinson BA, Dash ZV, et al. User manual for the FEHM application version 3.3.0. Los Alamos (USA): Los Alamos National Laboratory; 2015.

[23] Carey JW, Lewis K, Kelkar S, et al. Geomechanical behavior of wells in geologic sequestration. Energy Procedia. 2013;37:5642–5652.

[24] Dempsey D, Kelkar S, Pawar R. Passive injection: A strategy for mitigating reservoir pressurization, induced seismicity and brine migration in geologic CO_2 storage. Int J Greenhouse Gas Control. 2014;28:96–113.

[25] Bai M, Meng F, Elsworth D, et al. Analysis of stress-dependent permeability in nonorthogonal flow and deformation fields. Rock Mech Rock Eng. 1999;32:195–219.

[26] Lee HS, Cho TF. Hydraulic characteristics of rough fractures in linear flow under normal and shear load. Rock Mech Rock Eng. 2002;35:299–318.

[27] Warpinski NR, Abou-Sayed IS, Moschovidis Z. Hydraulic fracture model comparison study: complete results. Albuquerque (New Mexico, USA): Sandia National Laboratories; 1993.

[28] Dahi-Taleghani A, Olson JE. Numerical modeling of multistranded-hydraulic-fracture propagation: accounting for the interaction between induced and natural fractures. SPE J. 2011;16:575–581.
[29] Ribeiro LH, Sharma MM. A new 3D compositional model for hydraulic fracturing with energized fluids. SPE Prod Oper. 2013;28:259–267.
[30] Xu W, Thiercelin M, Walton I. Characterization of hydraulically-induced shale fracture network using an analytical/semi-analytical model. SPE 124697, 2009.
[31] Xu W, Le Calvez J, Thiercelin M. Characterization of hydraulically-induced fracture network using treatment and microseismic data in a tight-gas formation: a geomechanical approach. SPE 125237, 2009.
[32] Xu W, Thiercelin M, Ganguly U, et al. Wiremesh: a novel shale fracturing simulator. SPE 132218, 2010.
[33] Kresse O, Cohen C, Weng X, et al. Numerical modeling of hydraulic fracturing in naturally fractured formations. ARMA. 2011: 11–363.
[34] Dershowitz W, Ambrose R, Lim D, et al. Hydraulic fracture and natural fracture simulation for improved shale gas development. Paper presented at American Association of Petroleum Geologists Annual Convention and Exhibition; Houston, Texas, U.S.A., 10–13 April 2011.
[35] Meyer BR, Bazan LW. A discrete fracture network model for hydraulically induced fractures: theory, parametric and case studies. SPE. 2011;140514.
[36] Zyvoloski GA. FEHM: A control volume finite element code for simulating subsurface multi-phase multi-fluid heat and mass transfer. Los Alamos (USA): Los Alamos National Laboratory; 2007.
[37] Xu T, Sonnenthal E, Spycher N, et al. TOUGHREACT v3.0-OMP reference manual: a parallel simulation program for non-isothermal multiphase geochemical reactive transport. Berkeley: Earth Sciences Division, Lawrence Berkeley National Laboratory; 2014-a.
[38] Pruess K, Oldenburg C, Moridis G. TOUGH2 user's guide, version 2.0. Berkeley (USA): Earth Sciences Division, Lawrence Berkeley National Laboratory, University of California; 1999.
[39] Pruess K. ECO2N: a TOUGH2 fluid property module for mixtures of water NACL and CO_2. Berkeley (USA): Earth Sciences Division, Lawrence Berkeley National Laboratory, University of California; 2005.
[40] Doughty C, Pruess K. Modeling supercritical carbon dioxide injection in heterogeneous porous media. Vadose Zone J. 2004;3:837–847.
[41] Lasaga AC, Soler JM, Ganor J, et al. Chemical weathering rate laws and global geochemical cycles. Geochimica Cosmochimica Acta. 1994;58:2361–2386.
[42] Corey AT. The interrelation between gas and oil relative permeabilities. Producer's Monthly. 1954;19:38–41.
[43] Bertels SP, DiCarlo DA, Blunt MJ. Measurement of aperture distribution, capillary pressure, relative permeability, and in situ saturation in a rock fracture using computed tomography scanning. Water Resour Res. 2001;37:649–662.
[44] van Genuchten MT. A closed-form equation for predicting the hydraulic conductivity of unsaturated soils. Soil Sci Soc Am J. 1980;44:892–898.
[45] Schwartz MO. Modelling radionuclide transport in large fractured-media systems: the example of forsmark, Sweden. Hydrogeol J. 2012;20:673–687.
[46] Schwartz MO. Nuclear waste disposal – groundwater contamination in three dimensions. Beau Bassin (Mauritius): Scholar's Press; 2019; ISBN 978-613-8-90968-2.
[47] Pollyea RM, Rimstidt JD. Rate equations for modeling carbon dioxide sequestration in basalt. Appl Geochem. 2017;81:53–62.
[48] Reeder RJ, Dollase WA. Structural variation in the dolomite-ankerite solid-solution series: An X-ray, mössbauer, and TEM study. Am Mineral. 1989;74:1159–1167.
[49] Meunier A, Velde B. Solid solutions in I/S mixed-layer minerals and illite. Am Mineral. 1989;74:1106–1112.
[50] Knauss KG, Johnson JW, Steefel CI. Evaluation of the impact of CO_2, co-contaminant gas, aqueous fluid and reservoir rock interactions on the geologic sequestration of CO_2. Chem Geol. 2005;217:339–350.
[51] Palandri JL, Kharaka YK. A compilation of rate parameters of water-mineral interaction kinetics for application to geochemical modeling. Washington, D.C., U.S.A.: U.S. Geological Survey Open File Report 2004-1068; 2004.
[52] Oelkers EH, Gislason SR. The mechanism, rates, and consequences of basaltic glass dissolution: I. An experimental study of the dissolution rates of basaltic glass as a function of aqueous Al, Si and oxalic acid concentration at 25°C and pH = 3 and11. Geochimica Cosmochimica Acta. 2001;65:3671–3681.
[53] Blanc P, Lassin A, Piantone P. THERMODDEM a data base devoted to waste minerals. Orléans (France): BRGM; 2007. Available from: http://thermoddem.brgm.fr.
[54] Aradóttir ESP, Sonnenthal EL, Björnsson G, et al. Multidimensional reactive transport modeling of CO_2 mineral sequestration in basalts at the Hellisheidi geothermal field, Iceland. Int J Greenhouse Gas Control. 2012;9:24–40.
[55] Gislason SR, Broecker WS, Gunnlaugsson E, et al. Rapid solubility and mineral storage of CO_2 in basalt. Energy Procedia. 2014;63:4561–4574.
[56] Feiveson H, Mian H, Ramana MV, et al. Spent fuel from nuclear power reactors, 2011. Available from: http://fissilematerials.org/library/ipfm-spent-fuel-overview-june-2011.pdf.
[57] Windkraft-Journal. Der weltweit erste offshore-Windpark ohne Subventionen wird in den Niederlanden gebaut, 2018. [cited 2020 Aug 6]. Available from: https://www.windkraft-journal.de/2018/03/20.
[58] LAZARD. LAZARD's levelized cost of energy analysis - version 13.0, 2019. [cited 2020 Aug 6]. Available from: https://www.lazard.com.